Letter

Fluidity in domain walls in dilute ^{3}He-^{4}He films on graphite: Possible one-dimensional Fermi fluid and Dirac fermions in a helium film

Masashi Morishita *

Faculty of Pure and Applied Sciences, University of Tsukuba, Tsukuba, Ibaraki 305-8571, Japan

(Received 16 August 2022; revised 2 November 2022; accepted 23 December 2022; published 18 January 2023)

The heat capacity of a small number of ^{3}He atoms dissolved in a submonolayer ^{4}He film has been measured. The measured heat capacity is finite and suggests that ^{3}He atoms are mobile in an areal density regime higher than that of the $\sqrt{3} \times \sqrt{3}$ phase, where ^{4}He films are believed to be solid. At higher areal densities, the measured heat capacity is proportional to T^2 and depends on the number of ^{3}He atoms. These behaviors are anomalous to that of a two-dimensional Fermi fluid and cannot be explained by uniform melting of ^{4}He films. One possible explanation for these anomalous behaviors is that helium atoms exhibit fluidity only inside the domain walls of the adsorption structure, and the dissolved ^{3}He atoms gather in them and behave as a one-dimensional Fermi fluid or as Dirac fermions, depending on the structure of the domain walls. The behaviors of the measured heat capacity strongly suggest this possibility.

DOI: 10.1103/PhysRevB.107.L020505

The quantum properties of low-dimensional matter have attracted much attention in condensed matter physics. Graphene is one of the most fascinating and peculiar examples that can be treated as two-dimensional (2D) [1] because it exhibits novel and unique features, and studies on its properties and applications have evolved explosively in the last decade. A helium film adsorbed onto a graphite surface provides an almost ideal 2D system and exhibits a well-defined layer-by-layer structure [2]. Each layer is independent of the others and exhibits high flatness and uniformity. The ^{3}He atom has a nuclear spin of 1/2, and the ^{3}He solid film provides a 2D quantum spin system and has been investigated vigorously [3–5]. With an increase in areal density, their magnetism exhibits rather a complicated change [6–8] which has been discussed with the evolution of the adsorption structure [9,10]. On the other hand, information on the properties and adsorption structures of ^{4}He films is limited due to the lack of an appropriate method for their observation.

In this Letter, I report the results of heat capacity measurements of a small number of ^{3}He atoms dissolved into submonolayer ^{4}He films on graphite. The results strongly suggest that ^{3}He atoms are mobile in an areal density regime higher than that of the $\sqrt{3} \times \sqrt{3}$ phase, where ^{4}He films are believed to be solid. At higher areal densities the measured heat capacity is in proportion to the square of temperature. This anomalous temperature variation cannot be explained if ^{3}He atoms move around the entire surface of the graphite. At these areal densities, ^{4}He films are expected to have domain wall superstructures [11–14]. A possible explanation for these anomalous observations is that ^{4}He atoms in domain walls exhibit fluidity and that ^{3}He atoms gather into and move around only inside domain walls. Fluidity inside domain walls provides regular confined geometry with a width of atomic size for ^{3}He atoms. ^{3}He atoms can be expected to behave as a one-dimensional Fermi fluid or as Dirac fermions, depending on the structure of domain walls (striped or honeycomb).

The heat capacity measurement of dilute ^{3}He-^{4}He mixed films can be utilized to clarify the nature of ^{4}He films, and this approach was first adopted by Ziouzia *et al.* [15]. The heat capacity of ^{4}He films is very small [12,16] and gives very little information about the nature of ^{4}He films. A small number of ^{3}He atoms dissolve only into the top layer of a ^{4}He thin film. When the top layer of the ^{4}He film is a fluid, the ^{3}He atoms behave as a Fermi fluid and exhibit finite heat capacity, giving information about the ^{4}He film. On the other hand, when the ^{4}He film is solid, the dissolved ^{3}He atoms are almost localized and exhibit almost no heat capacity contribution.

The heat capacity is measured between 1 and 80 mK using the usual adiabatic heat-pulse method. The graphite substrate used in this work is Grafoil. The total surface area of the substrate is approximately 390 m^2. To ensure uniformity of the ^{3}He-^{4}He film, the following procedures are adopted in sample preparation. First, a sufficient amount of the sample ^{4}He is introduced into the sample cell to cover the heterogeneous surface of the Grafoil substrate. After the ^{4}He film is annealed by raising the temperature once, a designated amount of ^{3}He gas is introduced, and the sample film is annealed again. Typically, in a series of measurements, the amount of ^{3}He is fixed at some value which corresponds to areal densities ρ_3 of 0.1 or 0.2 nm^{-2}, while the amount of ^{4}He is gradually increased. Annealing is performed after the introduction of each sample over 6–8 h at a high temperature with a sample vapor pressure of around 500 Pa. After the annealing, the temperature is slowly decreased over 8–10 h until the vapor pressure becomes much less than 1 Pa. The vapor pressure is measured by an *in situ* pressure gauge. Other experimental details are similar to those in my previous works [17,18].

*morishita.masashi.ga@u.tsukuba.ac.jp

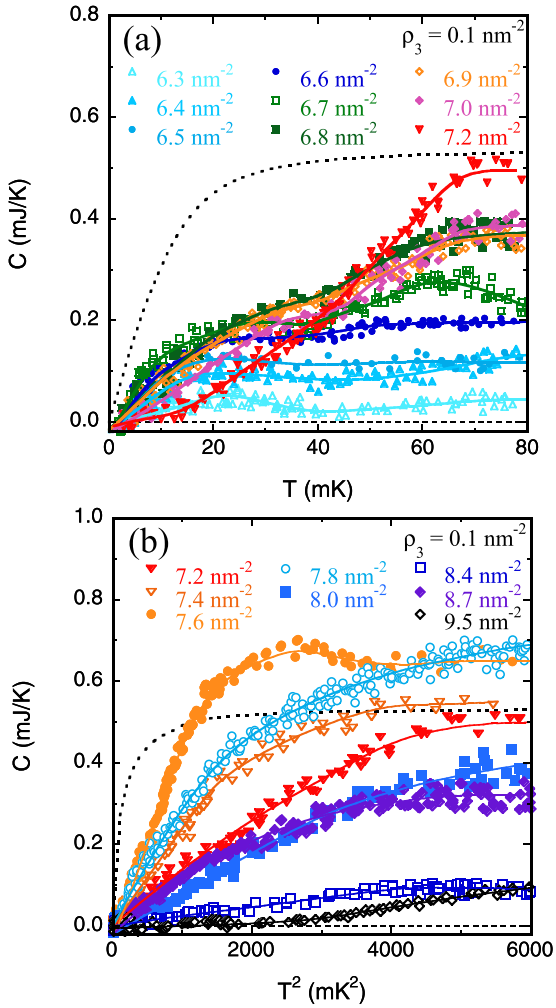

FIG. 1. Measured heat capacity of dilute ^{3}He-^{4}He mixed films is plotted for select areal densities (a) below 7.2 nm^{-2} as a function of T and (b) above 7.2 nm^{-2} as a function of T^2. Numbers in the legend indicate the total areal density of ^{3}He and ^{4}He (ρ_{total}), and here the areal density of ^{3}He is 0.1 nm^{-2}. The dotted lines indicate the expected heat capacity of an ideal 2D Fermi gas of 0.1 nm^{-2}, and the dashed lines indicate the origin of the vertical axes. The solid lines are guides for the eye.

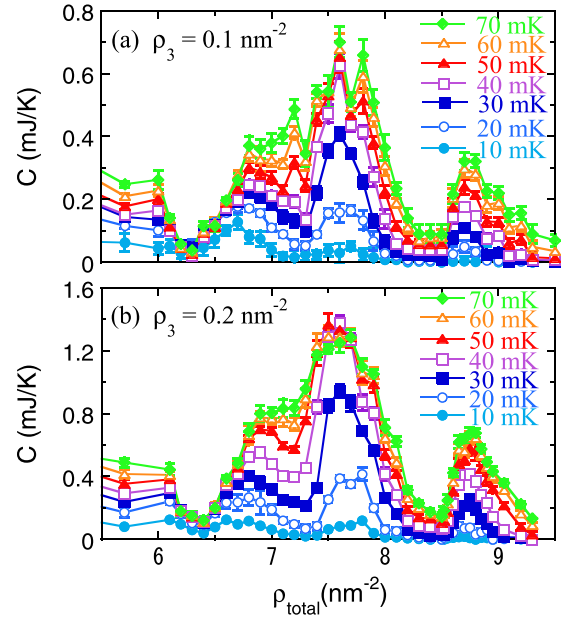

FIG. 2. Isotherms of the measured heat capacity of dilute ^{3}He-^{4}He mixed films for (a) $\rho_3 = 0.1$ and (b) $\rho_3 = 0.2$ nm^{-2}. The finite heat capacities above the areal density of the $\sqrt{3} \times \sqrt{3}$ phase (6.4 nm^{-2}) strongly suggest that ^{3}He atoms are mobile even at these areal densities. The almost linear increases at high temperatures just above 6.4 nm^{-2} indicate that the number of mobile ^{3}He atoms increase linearly with increasing total areal density.

The measured heat capacities C of submonolayer dilute ^{3}He-^{4}He mixed films at select areal densities are shown in Fig. 1 as a function of temperature T or of the square of temperature T^2 (see the Supplemental Material [19], Sec. 1, for the temperature variations with expanded scales at low temperatures). The isotherms of measured heat capacities are shown in Fig. 2. As reported elsewhere [20], with increasing areal density from the fluid phase and approaching an areal density of 6.3 nm^{-2}, the measured heat capacity approaches zero. This value of areal density corresponds to that of the $\sqrt{3} \times \sqrt{3}$ phase, and this behavior can be attributed to the solidification of the ^{3}He-^{4}He film into the $\sqrt{3} \times \sqrt{3}$ phase. However, with a further increase of the areal density, the measured heat capacity increases and becomes finite, as shown in Figs. 1 and 2. This behavior suggests that the ^{3}He atoms are mobile, although in this areal density regime the ^{4}He film is believed to be solid. Furthermore, at areal densities higher than 7.2 nm^{-2} the measured heat capacity is proportional to T^2 [as shown in Fig. 1(b)], and the magnitude of the measured heat capacity is almost proportional to the number of ^{3}He atoms (as shown below in Fig. 5). The heat capacity of a 2D Fermi fluid is proportional to T at low temperatures, and its slope is independent of the number density of particles. Therefore, ^{3}He atoms dissolved in submonolayer ^{4}He films at these areal densities cannot be considered a Fermi fluid, and uniform melting of ^{4}He films cannot explain the observations.

There are some candidates for the possible origins of the observed anomalous heat capacity. The T^2 variation is reminiscent of the 2D phonon contribution. However, the heat capacities of pure ^{4}He films, whose origins can be attributed to phonons, are far smaller than the measured ones here [12,16,21]. In other words, the magnitude of the observed heat capacity can be explained only by the nonrealistic Debye temperature of the order of 1 mK. The ^{3}He nuclear spin contribution can also be excluded because the interactions between ^{3}He nuclear spins should be extremely weak in the context of this experiment, and furthermore, entropy changes calculated from measured heat capacities are much larger than the expected change, $N_3 k_B \ln 2$, where N_3 is the number of ^{3}He atoms. A film consisting of a ^{3}He-^{4}He mixture can exhibit phase separation into ^{3}He-rich and ^{4}He-rich phases, and the mixing of these phases with increasing temperature is also a candidate for the origin of the observed heat capacity. However, the heat capacity contribution from the mixing should be independent of the amount of ^{3}He. The dependence of the observed heat capacity on the ^{3}He amount can exclude this possibility.

Helium films are thought to solidify with the important contribution of hard-core repulsion between helium atoms and the corrugation of the adsorption potential [22–24]. At higher areal densities, a plausible structure is the domain wall (DW) superstructure. DWs exhibit two different structures, namely, the striped and honeycomb DW structures. The DW structures have been discussed for and observed in many adsorbed systems on graphite. For the ^{3}He monolayer film, the areal density evolution of the DW structures has been discussed according to Monte Carlo calculations [9,10]. Also for a ^{4}He monolayer film on graphite, DW structures have been theoretically predicted [11,14] and proposed according to experimental observations [12]. In the DWs, the role of the corrugation in solidification is less important, and ^{4}He could exhibit fluidity. The situation is somewhat similar to the possible fluidity inside dislocations and grain boundaries in hcp ^{4}He in relation to its observed "supersolid"-like behavior [25]. If DWs exhibit fluidity, ^{3}He atoms should crowd onto the DWs to reduce their zero-point energies and move about in the DWs. Therefore, confined geometries with a width of atomic size are provided for ^{3}He atoms. Although the structures of dislocations and grain boundaries in hcp ^{4}He are irregular, the DWs are arranged regularly, and the behaviors of ^{3}He atoms dissolved in them can be expected to reflect the regular structure.

In the case of striped DW structures (which appear in a lower areal density regime), ^{3}He atoms should travel in one-dimensional (1D) space and behave as a 1D Fermi fluid. Hence, ^{3}He atoms dissolved in striped DWs in a ^{4}He film are a possible candidate for a Tomonaga-Luttinger liquid, although evidence for this has yet to be obtained in heat capacity measurements.

In the case of honeycomb DW structures (which appear in a higher areal density regime), ^{3}He atoms should travel in honeycomb lattices. Their degree of freedom is similar to that of electrons in graphene. In graphene, electrons behave as massless Dirac fermions, and their dispersion near the Dirac points is linear [1]. Similar behaviors have been observed in an ultracold gas of potassium atoms in honeycomb lattices [26] and in carbon monoxide molecules in a hexagonal pattern [27]. ^{3}He atoms in the honeycomb DWs of ^{4}He films are similarly expected to have linear dispersion. In this case, their heat capacity is expected to be proportional to T^2, and observed anomalous T^2 variation at high areal densities can be explained. An almost T^2 dependence has been reported in the heat capacity measurement of a multilayered organic material, in which massless Dirac fermions are expected [28].

The linear dispersion relation of graphene is usually explained using the tight-binding approach [1,29], which is not adequate for the ^{3}He atoms dissolved into a ^{4}He fluid. However, it has been revealed that the tight-binding nature is not necessary for the appearance of the linear dispersion relation. Lomer discussed the band structure of graphene using a group-theoretical treatment [30]. Park and Louie showed that the Dirac fermion nature can be generated within an independent particle picture [31]. Geng *et al.* found that the linear dispersion relation appears in discretized tight-binding models, although the Fermi level does not coincide with the Dirac point [32,33].

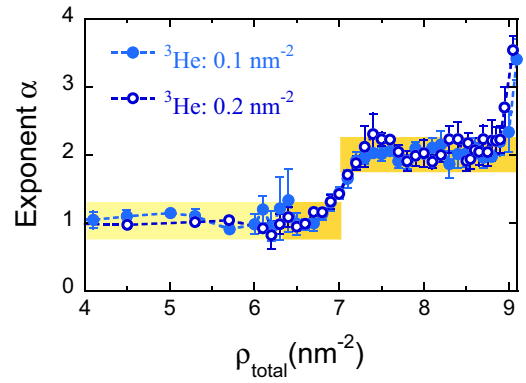

FIG. 3. Exponent of measured heat capacity of dilute ^{3}He-^{4}He mixed films in a low-temperature regime. The colored rectangles are guides for the eye. The sudden change at around 7.0 nm^{-2} strongly suggests the structural phase transition between striped and honeycomb domain wall structures.

The exponent α of the measured heat capacity, which is obtained by fitting the measured values with $C \propto T^\alpha$ in the low-temperature regime, where the convex is not upward in a T-C plot, is shown in Fig. 3. The error bars indicate the uncertainties owing to the choice of the temperature range used for the fit (see the Supplemental Material [19], Sec. 2, for a detailed procedure to obtain the exponents). Results shown in Fig. 3 include those of films in the fluid-solid coexistence region in a low areal density regime ($4.0 \leqslant \rho_{\text{total}} \leqslant 6.4$ nm^{-2}), where some fraction of ^{3}He atoms dissolves into the fluid phase and behaves as 2D Fermi liquids. The rather sudden change from T-linear to T^2 behavior at around 7.0 nm^{-2} can be attributed to the structural phase transition between the striped and honeycomb DW structures. In the case of a submonolayer pure ^{3}He film, the structural phase transition between striped and honeycomb DW structures is predicted to occur around 6.8 nm^{-2} [10]. This value is similar to that of the areal density where the exponent of the measured heat capacity suddenly changes, although the masses and the quantum statistics are different between ^{3}He and ^{4}He.

Next, let us pay attention to the behaviors in a high-temperature regime. The heat capacity of a 1D Fermi fluid approaches $N_3 k_B/2$ at the high-temperature limit. In Fig. 1, the dotted lines indicate the expected behavior for a 2D Fermi gas which saturates to $N_3 k_B$. In Fig. 1(a), the measured heat capacities tend to saturate to $N_3 k_B/2$ at high temperatures. The observed smaller values can be attributed to the finite solubility of ^{3}He in domain walls. That is, some fraction of ^{3}He atoms dissolves in $\sqrt{3} \times \sqrt{3}$ domains and is localized. The ^{3}He solubility in DWs does not depend on the total areal density, and the total length of DWs increases linearly with the total areal density. Thus, the number of ^{3}He atoms dissolved in DWs increases linearly with the total areal density. The almost linear increases just above 6.4 nm^{-2} in the high-T isotherms in Fig. 2 are consistent with this expectation. More precisely, for $\rho_3 = 0.1$ nm^{-2} and $\rho_3 = 0.2$ nm^{-2}, the number of ^{3}He atoms increases linearly up to 6.8 and 6.9 nm^{-2}, respectively. These similar limits of areal densities indicate that ^{3}He solubility depends on the ^{3}He dose, which is unexpected. However, the spreading pressure depends on the ^{3}He fraction.

Therefore, an increase in the ^{3}He solubility in DWs with the increase of the ^{3}He fraction cannot be ruled out. On the other hand, at areal densities between 6.7 and 6.9 nm^{-2}, the measured heat capacities tend to saturate once to $N_3k_B/2$ at around 40 mK but increase further at higher temperatures, as shown in Fig. 1. The DW structure may change from striped to honeycomb with increasing temperature near the critical areal density. If the heat capacity contribution of $N_3k_B/2$ comes from ^{3}He atoms traveling in the DWs, the ^{3}He solubility in DWs reaches several percent or more. These values are much larger than the solubility in the fluid phase of the second atomic layer of ^{4}He films, which is reported to be less than 2% [15]. In the case of the fluid phase, ^{3}He atoms in the phase-separated condensed phase are also mobile, but in the case of the DW structure, ^{3}He atoms in the domains are localized. The magnitudes of the zero-point energy are very different from each other, which explains the observed large solubility in DWs.

With increasing temperature, the heat capacity of a 2D Fermi gas with linear dispersion is expected to overshoot once and then decrease and saturate to $2Nk_B$, which is twice the expected value for an ordinary 2D Fermi gas. The measured heat capacities appear to approach N_3k_B, and not $2N_3k_B$, with a rather large distribution. The thermal de Broglie length of ^{3}He atoms at 10 mK is about 10 nm, which is similar to the platelet size of Grafoil [34]; at 100 mK it is several nanometers, which is similar to the lattice constants of the honeycomb domain wall structures. Therefore, in a sufficiently low temperature regime, ^{3}He atoms can be affected by the honeycomb structures. However, at higher temperatures, ^{3}He atoms should behave as ordinary 2D fermions, and their heat capacity should approach N_3k_B. The excess observed at around 7.6 nm^{-2} can be explained by the prospect that the heat capacity exceeds N_3k_B before the ^{3}He atoms lose the nature of Dirac fermions, or the linear dispersion, with increasing temperature. Conversely, the observation of the excess supports the peculiarity of this system. Indeed, at these areal densities, the measured heat capacities tend to decrease and seemingly approach N_3k_B at high temperatures.

The slope of the heat capacity of a 1D Fermi gas at low temperatures is $\gamma = g^2{k_B}^2mL^2/3\hbar^2N$, where g is the number of degrees of spin freedom, m is the mass, L is the system length, and N is the number of Fermi particles. The estimated changes in γ are shown in Fig. 4 using this formula for the cases with $\rho_3 = 0.1$ and 0.2 nm^{-2}. The ^{3}He concentration in DWs is low, and the increases in the effective mass due to the correlation are neglected here. Although the hydrodynamic mass m_H must be considered in the case of ^{3}He atoms in ^{4}He, the magnitude of m_H in the case of submonolayer films has not yet been determined. Therefore, the reported value of $m_H/m \approx 1.4$ for the case of four atomic layers of ^{4}He [35] is adopted. The length of the DWs, which corresponds to L, increases linearly with the total areal density and can be estimated from the total areal density. The DW structure cannot appear on the heterogeneous surface of the Grafoil substrate. The fraction of the homogeneous surface of the Grafoil substrate used in this work was estimated to be approximately 70% of the total surface area [18]. Because the solubility of ^{3}He is limited, N can differ from the number of dosed ^{3}He atoms. N is projected to rise linearly with L, eventually reaching the number of dosed ^{3}He atoms at some areal density ρ_0. As mentioned above, $\rho_0 \approx 6.8$ nm^{-2} for $\rho_3 = 0.1$ nm^{-2}, and $\rho_0 \approx 6.9$ nm^{-2} for $\rho_3 = 0.2$ nm^{-2}. The dashed line in Fig. 4 is the estimated behavior for $\rho_3 = 0.1$ nm^{-2} and the solid line is for $\rho_3 = 0.2$ nm^{-2}. The slopes of the measured heat capacity, which are obtained by fitting the measured heat capacity with $C = \gamma T$ at low temperatures (typically below 20 mK), are also shown in Fig. 4. The estimated behaviors reproduce the observations semiquantitatively without adjustable parameters. Although the observed γ values appear to not depend on the ^{3}He dose and the estimation cannot reproduce this behavior, the increase in the effective mass m^* with increasing ^{3}He quantity could explain this discrepancy. The estimated behavior for $\rho_3 = 0.2$ nm^{-2} assuming $m^* = 1.3m_H$ is also shown with the dashed-and-dotted line in Fig. 4. The decreases in the slopes of the measured heat capacity at high areal densities can be attributed to the coexistence of honeycomb DWs.

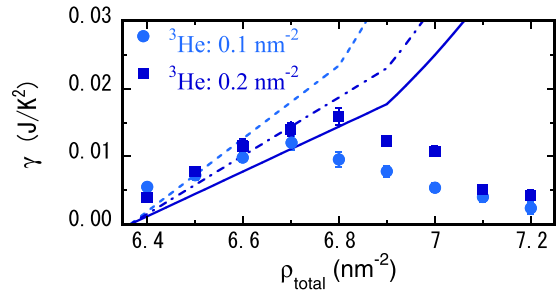

FIG. 4. Areal density variation of the slope of the measured heat capacity. The dashed, solid, and dashed-and-dotted lines are expected behaviors for the striped domain wall structure with $\rho_3 = 0.1$ nm^{-2} and $\rho_3 = 0.2$ nm^{-2}, with assumptions described in the text.

The coefficients of the T^2 term γ_2 is obtained by fitting the measured values with $C = \gamma_2T^2$ in a low-temperature regime (typically below 30 mK). As shown in Fig. 5, the T^2 term disappears at around 9.1 nm^{-2}. Further, as depicted in Fig. 3, the T^2 term disappears at approximately 8.8 nm^{-2}. These

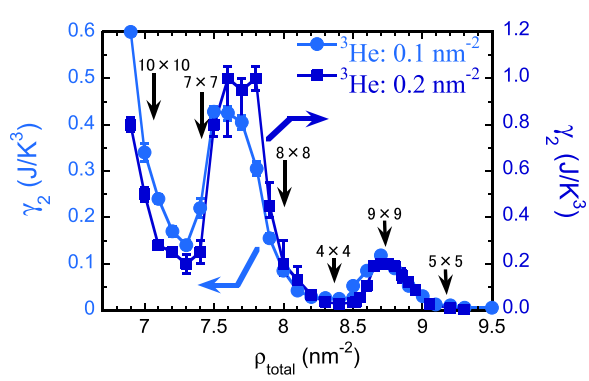

FIG. 5. Areal density variation of the coefficient of the T^2 term of the measured heat capacities. The scale of the vertical axis for $\rho_3 = 0.1$ nm^{-2} is shown on the left, and that for $\rho_3 = 0.2$ nm^{-2} is on the right. These scales differ from each other according to the amount of ^{3}He. The arrows indicate the areal densities where the honeycomb domain wall structure with displayed periodicity has a regular hexagonal structure.

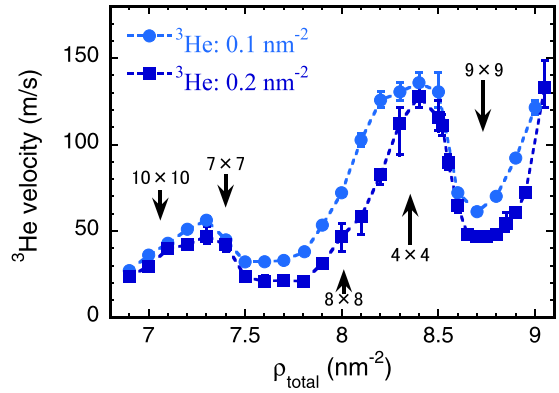

FIG. 6. Areal density variation of the velocity of ^{3}He atoms estimated from the measured heat capacity, assuming ^{3}He atoms behave as Dirac fermions. The increase observed at areal densities above 8.6 nm^{-2} may be incorrect due to the coexistence of the domain wall structure and incommensurate solid phase.

observations indicate that honeycomb DW structures survive up to considerably higher areal densities than the expected values: 7.9 nm^{-2} from heat capacity measurements [16] and 8.4 nm^{-2} from theoretical simulations [14].

If ^{3}He atoms behave as Dirac fermions, their speeds are the same because they exhibit linear dispersion. The speed of ^{3}He atoms v_3 can be estimated from γ_2 with the formula $v_3 = [9g\zeta(3)k_B^3 A/2\pi\hbar\gamma_2]^{1/2}$, assuming that interactions between ^{3}He atoms are weak, where $g = 4$ is the number of degrees of degeneracy, $\zeta(3)$ is the Riemann zeta function, and A is the surface area for the honeycomb structure [36]. The estimated velocities are shown in Fig. 6 as a function of total areal density. The estimated velocity has maxima at around 8.4 nm^{-2}, and it is much higher than the Fermi velocity in ^{3}He films behaving as a 2D Fermi fluid. At 8.4 nm^{-2}, the honeycomb DW structure is expected to have a regular structure with a periodicity of 4×4 versus the periodicity of the hollow sites of graphite. This structure has the smallest periodic length within honeycomb DW structures. Therefore, the honeycomb structure can be defined very well here, although the platelet size of Grafoil is small. The maximum value of v_3 at this areal density can be attributed to this reason.

The magnitude of v_3 appeared to saturate at approximately 130 m/s. This behavior suggests the existence of a critical velocity. Although one possible origin is the critical velocity of the 2D superfluid ^{4}He, measurements with smaller amounts of ^{3}He are desirable.

In summary, the heat capacity of a small number of ^{3}He atoms dissolved in a submonolayer ^{4}He film on graphite was measured. The observed behaviors suggest the nature of ^{3}He atoms is that of 1D fermions in the low areal density regime and that of Dirac fermions in the higher areal density regime. These results strongly suggest that the films exhibit fluidity in the domain walls. The origin of the fluidity and natures of ^{3}He and also ^{4}He atoms in domain walls must be understood further with successive research.

The author acknowledges stimulating discussions with T. Takagi, T. Minoguchi, M. Oshikawa, C. Geng, Y. Hatsugai, and Y. Ootuka. This research was supported by the Cryogenics Division, Research Facility Center for Science and Technology, University of Tsukuba.

[1] A. H. Castro Neto, F. Guinea, N. M. R. Peres, K. S. Novoselov, and A. K. Geim, Rev. Mod. Phys. **81**, 109 (2009).
[2] G. Zimmerli, G. Mistura, and M. H. W. Chan, Phys. Rev. Lett. **68**, 60 (1992).
[3] H. Godfrin, Prog. Low. Temp. Phys. **14**, 213 (1995).
[4] H. Godfrin and R. E. Rapp, Adv. Phys. **44**, 113 (1995).
[5] H. Fukuyama, J. Phys. Soc. Jpn. **77**, 111013 (2008).
[6] D. S. Greywall, Phys. Rev. B **41**, 1842 (1990).
[7] H. Godfrin, K. D. Morhard, R. E. Rapp, and Y. M. Bunkov, Phys. B (Amsterdam, Neth.) **194–196**, 675 (1994).
[8] H. Ikegami, K. Obara, D. Ito, and H. Ishimoto, Phys. Rev. Lett. **81**, 2478 (1998).
[9] M. Morishita and T. Takagi, Phys. Rev. Lett. **87**, 185301 (2001).
[10] M. Morishita and T. Takagi, Phys. B (Amsterdam, Neth.) **329–333**, 137 (2003).
[11] T. Halpin-Healy and M. Kardar, Phys. Rev. B **34**, 318 (1986).
[12] D. S. Greywall, Phys. Rev. B **47**, 309 (1993).
[13] P. Mohandas, C. P. Lusher, V. A. Mikheev, B. Cowan, and J. Saunders, J. Low Temp. Phys. **101**, 481 (1995).
[14] P. Corboz, M. Boninsegni, L. Pollet, and M. Troyer, Phys. Rev. B **78**, 245414 (2008).
[15] F. Ziouzia, J. Nyéki, B. Cowan, and J. Saunders, Phys. B (Amsterdam, Neth.) **329–333**, 252 (2003).
[16] D. S. Greywall and P. A. Busch, Phys. Rev. Lett. **67**, 3535 (1991).
[17] M. Morishita, J. Low Temp. Phys. **171**, 664 (2013).
[18] M. Morishita, H. Nagatani, and H. Fukuyama, Phys. Rev. B **65**, 104524 (2002).
[19] See Supplemental Material at http://link.aps.org/supplemental/10.1103/PhysRevB.107.L020505 for the temperature variations with expanded scales at low temperatures and for a detailed procedure to obtain the exponents.
[20] M. Morishita, J. Low Temp. Phys. **183**, 245 (2016).
[21] M. Morishita, J. Low Temp. Phys. **187**, 453 (2017).
[22] A. Casey, H. Patel, J. Nyéki, B. P. Cowan, and J. Saunders, Phys. Rev. Lett. **90**, 115301 (2003).
[23] D. S. Hirashima, T. Momoi, and T. Takagi, J. Phys. Soc. Jpn. **72**, 1446 (2003).
[24] Y. Matsumoto, D. Tsuji, S. Murakawa, H. Akisato, H. Kambara, and H. Fukuyama, J. Low Temp. Phys. **138**, 271 (2005).
[25] M. H. W. Chan, R. B. Hallock, and L. Reatto, J. Low Temp. Phys. **172**, 317 (2013).
[26] L. Tarruell, D. Greif, T. Uehlinger, G. Jotzu, and T. Esslinger, Nature (London) **483**, 302 (2012).
[27] K. K. Gomes, W. Mar, W. Ko, F. Guinea, and H. C. Manoharan, Nature (London) **483**, 306 (2012).
[28] T. Konoike, K. Uchida, and T. Osada, J. Phys. Soc. Jpn. **81**, 043601 (2012).

[29] P. R. Wallace, Phys. Rev. **71**, 622 (1947).
[30] W. M. Lomer, Proc. R. Soc. London, Ser. A **227**, 330 (1954).
[31] C.-H. Park and S. G. Louie, Nano Lett. **9**, 1793 (2009).
[32] C. Geng, M. Morishita, and M. Oshikawa (unpublished).
[33] C. Geng, M.S. thesis, Spectrum of thin helium-mixture films with a honeycomb structure, University of Tokyo, 2018.
[34] R. J. Birgeneau, P. A. Heiney, and J. P. Pelz, Phys. B (Amsterdam, Neth.) **109–110**, 1785 (1982).
[35] M. Dann, J. Nyéki, B. P. Cowan, and J. Saunders, Phys. Rev. Lett. **82**, 4030 (1999).
[36] O. Vafek, Phys. Rev. Lett. **98**, 216401 (2007).